Characterization of *samhd1* Morphant Zebrafish Recapitulates Features of the Human Type I Interferonopathy Aicardi-Goutières Syndrome

Paul R. Kasher, Emma M. Jenkinson, Valérie Briolat, David Gent, Catherine Morrissey, Leo A. H. Zeef, Gillian I. Rice, Jean-Pierre Levraud and Yanick J. Crow

J Immunol 2015; 194:2819-2825; Prepublished online 11 February 2015;
doi: 10.4049/jimmunol.1403157
http://www.jimmunol.org/content/194/6/2819

The Journal of Immunology is published twice each month by
The American Association of Immunologists, Inc.,
1451 Rockville Pike, Suite 650, Rockville, MD 20852

Print ISSN: 0022-1767 Online ISSN: 1550-6606.

Characterization of *samhd1* Morphant Zebrafish Recapitulates Features of the Human Type I Interferonopathy Aicardi-Goutières Syndrome

Paul R. Kasher,* Emma M. Jenkinson,* Valérie Briolat,[†,‡] David Gent,* Catherine Morrissey,* Leo A. H. Zeef,[§] Gillian I. Rice,* Jean-Pierre Levraud,[†,‡] and Yanick J. Crow*,[¶]

In humans, loss of function mutations in the *SAMHD1* (*AGS5*) gene cause a severe form of Aicardi-Goutières syndrome (AGS), an inherited inflammatory-mediated encephalopathy characterized by increased type I IFN activity and upregulation of IFN-stimulated genes (ISGs). In particular, SAMHD1-related AGS is associated with a distinctive cerebrovascular pathology that commonly leads to stroke. Although inflammatory responses are observed in immune cells cultured from *Samhd1* null mouse models, these mice are physically healthy, specifically lacking a brain phenotype. We have investigated the use of zebrafish as an alternative system for generating a clinically relevant model of SAMHD1-related AGS. Using temporal gene knockdown of zebrafish *samhd1*, we observe hindbrain ventricular swelling and brain hemorrhage. Furthermore, loss of *samhd1* or of another AGS-associated gene, *adar*, leads to a significant upregulation of innate immune-related genes and an increase in the number of cells expressing the zebrafish type I IFN *ifnphi1*. To our knowledge, this is the first example of an in vivo model of AGS that recapitulates features of both the innate immune and neurological characteristics of the disease. The phenotypes associated with loss of *samhd1* and *adar* suggest a function of these genes in controlling innate immune processes conserved to zebrafish, thereby also contributing to our understanding of antiviral signaling in this model organism. ***The Journal of Immunology*****, 2015, 194: 2819–2825.**

Aicardi-Goutières syndrome (AGS) is a genetically determined inflammatory-mediated encephalopathy characterized by an upregulation of type I IFN activity and the increased expression of IFN-stimulated genes (ISGs) (1, 2). Mutations in seven genes are responsible for the AGS1-7 subtypes (3–7). A current hypothesis suggests a common role for these genes in the metabolism and signaling of endogenously derived nucleic acids. The *SAMHD1* (AGS5) gene encodes a protein that has recently been shown to function as an HIV-1 restriction factor, capable of inhibiting early stage viral DNA synthesis by depleting the intracellular deoxyribonucleotide triphosphate pool (8, 9). It has been proposed that in SAMHD1-related AGS (AGS5), loss of SAMHD1 function leads to cytoplasmic accumulation of DNA derived from the reverse transcription of endogenous retroelements, which in turn induces an IFN response. Clinically, AGS5 differs from other AGS subtypes in that many patients demonstrate a distinct cerebral vasculopathy (10–13). Remarkably, this vascular phenotype can manifest as both stenotic (vessel narrowing, leading to a moyamoya appearance) and aneurysmal (vessel bulging) disease, which carry a high risk of intracerebral hemorrhage and stroke. The pathological basis of this phenotype is predicted, but not proven, to relate to a discrete role for SAMHD1 in blood vessel homeostasis via an innate immune-mediated mechanism.

Recently, *Samhd1* knockout mouse models have been generated (14, 15). Although cell and tissue-specific phenotypes associated with increased IFN signaling were observed, these mice were healthy and lacked any overt brain or cerebrovascular phenotype. Thus, there remains a requirement for a clinically relevant in vivo model of defective SAMHD1 activity. The use of zebrafish is emerging as a powerful tool to study the immune system (16). During the first 3 weeks of life, zebrafish exclusively demonstrate features of an innate (rather than adaptive) immune response. Therefore, during early development, innate immunity can be investigated in the absence of T and B cell activity (17). Characterization of the innate immune signaling repertoire in zebrafish is incomplete. However, it has been shown that antiviral responses in zebrafish demonstrate transcriptional overlap with those defined in mammals (18). Using a temporal gene knockdown approach, we have generated a zebrafish model of *samhd1* deficiency. We observe cerebrovascular abnormalities that are associated with increased transcription of innate immune-responsive genes and an upregulation of *ifnphi1*, thereby apparently phenocopying AGS5.

*Manchester Centre for Genomic Medicine, Institute of Human Development, Faculty of Medical and Human Sciences, University of Manchester, Manchester M13 9WL, United Kingdom; [†]Institut Pasteur, Macrophages et Développement de l'Immunité, F-75015 Paris, France; [‡]Centre National de la Recherche Scientifique, Unité de Recherche Associée 2578, F-75015 Paris, France; [§]Faculty of Life Sciences, University of Manchester, Manchester M13 9PT, United Kingdom; and [¶]Laboratory of Neurogenetics and Neuroinflammation, Imagine Institute, Necker Hospital for Sick Children, 75015 Paris, France

Received for publication December 19, 2014. Accepted for publication January 15, 2015.

This work was supported by the Newlife Foundation, the Natalie Kate Moss Trust, the European Research Council (GA 309449: fellowship to Y.J.C.), and state subsidies managed by the National Research Agency (France) under the "Investments for the Future" program bearing the reference ANR-10-IAHU-01 and the "Zebraflam" program bearing the reference ANR-10-MIDI-009.

Address correspondence and reprint requests to Dr. Paul R. Kasher, Manchester Centre for Genomic Medicine, Institute of Human Development, Faculty of Medical and Human Sciences, 1st Floor Offices, AV Hill Building, University of Manchester, Oxford Road, Manchester M13 9PT, U.K. E-mail address: paul.kasher@manchester.ac.uk

The online version of this article contains supplemental material.

Abbreviations used in this article: AGS, Aicardi-Goutières syndrome; AGS5, SAMHD1-related AGS; ATG, translation start codon; dpf, d postfertilization; ISG, IFN-stimulated gene; IQR, interquartile range; MO, morpholino; QRT-PCR, quantitative real-time PCR; RQ, relative quantification; WT, wild type.

We propose that zebrafish may represent a novel in vivo system for studying the relationship between IFN signaling and a loss of SAMHD1 activity.

Materials and Methods

Zebrafish

Adult and larval zebrafish husbandry was approved by The University of Manchester Ethical Review Board and all experiments were performed in accordance with U.K. Home Office regulations. Embryos generated from a wild type (WT) AB zebrafish cross were used for morpholino (MO) characterization and gene expression analyses. Brain hemorrhage analyses were performed on embryos harvested from a double transgenic (*fli1a*:GFP)^{y1} / (*gata1a*:DsRed)^{sd2} adult zebrafish cross (19, 20), hereafter referred to as *fli:*GFP/*gata1:*DsRed. The (*ifnphi1*:mcherry)^{ip1} transgenic reporter line was used for *ifnphi1* expression analyses (21). Fertilized embryos were collected and staged according to standard guidelines (22).

Morpholinos

Two MOs were designed and synthesized (Gene Tools, Philomath, OR) for inhibition of the *samhd1* gene (*samhd1* translation start codon [ATG], 5′-GCCGTTTAATCCGGTTCTCCATGGT-3′; *samhd1* exon 4 splice donor, 5′-GCTCTCGGCTGTGAACGTACCCTAT-3′), as well as for the *adar* gene (*adar* ATG, 5′-AATTCCCTCCTCTACCTCTGCTCAT-3′; *adar* exon 4 splice donor, 5′-ACCTTGGAACGCATTTTACCGTGGA-3′). Fertilized embryos were injected with between 3.2 and 4.0 ng for both *samhd1* MOs and 0.8 ng and 8.0 ng for the *adar* ATG and splice MO, respectively. The sequence and injection dosages for the *cecr1* ATG MO have been published elsewhere (23). Standard control MOs provided by Gene Tools were also used. MO microinjection was performed as described previously (24).

Reverse transcriptase PCR

To assess efficiency of the splice MOs, total RNA was extracted as described previously (24). cDNA was synthesized from 400 ng RNA using the High Capacity RNA to cDNA Kit (Life Technologies). RT-PCR was performed using primers designed to flank exon 4 of the *samhd1* cDNA transcript (forward: 5′-CCTGCTGTGTCTGACTGAGG-3′; reverse: 5′−CAAATCATGGCACAATCCAG-3′) to generate a WT amplicon of 394 bp; and primers designed to flank exon 4 of the *adar* cDNA transcript (forward: 5′-AGATGGTCGCAGGTTTCCAG-3′; reverse: 5′−CTCTTTCACAGCCTCCTCCG-3′) to generate a WT amplicon of 427 kb.

Western blotting

For zebrafish protein lysates, embryos were pooled into groups of n = 40–60, dechorionated and deyolked (deyolking buffer: 55 mM NaCl, 1.8 mM KCl, 1.25 mM $NaHCO_3$), and subsequently washed (postdeyolking wash buffer: 110 mM NaCl, 3.5 mM KCl, 2.7 mM $CaCl_2$, 10 mM TrisHCl, pH 8.5). Embryos were then homogenized and lysed in EDTA plus RIPA buffer containing protease inhibitors (Roche). Whole-cell lysates from control and *SAMHD1* null AGS5 patient (c.1-6085_c.208+2691del hom) (2) lymphoblastoid cell lines were prepared as described previously (7). Western blotting was performed as described previously (7) using an anti-human SAMHD1 polyclonal Ab (Abcam; ab67820). An anti-human total-p44/42 MAPK (ERK1/2) Ab was used as a loading control (Cell Signaling Technology; no. 9102).

SAMHD1 cloning and in vitro transcription

Full-length human *SAMHD1* cDNA had been previously cloned into a pGEM-T easy vector (5). The expression cassette was excised using *Eco*R1 and subsequently ligated into pCS2+. In vitro transcription was performed using SP6 mMESSAGE mMACHINE (Life Technologies) following Not1 linearization. For the phenotypic rescue experiments, 100 pg of *SAMHD1* mRNA was injected alone as a control, or in combination with the *samhd1* ATG MO.

Taqman quantitative real-time PCR

Total RNA was extracted from n = 50–100 embryos at 4 d postfertilization (dpf) as described previously (24). cDNA was synthesized from 400 ng RNA using the High Capacity RNA to cDNA kit (Life Technologies). Quantitative real-time PCR (QRT-PCR) analysis was performed using the TaqMan Universal PCR Master Mix (Applied Biosystems). The relative abundance of target transcripts, measured using Taqman probes for *cebpb* (dr03201503_s1), *cxc46* (custom design; see Supplemental Fig. 1), *irf1b* (dr03151900_g1), *irf7* (dr03081134_g1), *isg15* (custom design; see Supplemental Fig. 1), *junbb* (dr03203565_s1), *mmp9* (dr03139883_g1), *socs3b* (dr03203997_s1) and *stat1b* (dr03151121_m1), was normalized to the expression of *hprt1* (dr03095131_g1). Gene expression fold changes were calculated using Applied Biosystems StepOne Software V2.1 and Applied Biosystems Data Assist Software V3.01. Fold change values for each gene were plotted against each morphant group using GraphPad Prism version 5.0 and defined as the relative quantification (RQ). Column statistics were used to generate the median RQ values for each morphant group for the nine target genes pooled together (7).

Flow cytometry

Morphant and control *ifnphi1:*mCherry transgenic embryos and non-transgenic embryos were harvested at 4 dpf (n = 40–60 embryos). Whole embryos were enzymatically dissociated using a 10 X Tryple (Life Technologies) and collagenase–dispase (Roche) mixture. Samples were incubated for 1 h at 28.5°C and triturated at regular intervals. Single-cell suspensions were analyzed using a BD Biosciences LSRFortessa cell analyzer running Diva 8.1 software. The samples were gated using FS-H Vs FS-A (forward scatter height versus forward scatter area) to select single cells and then on forward scatter versus side scatter to exclude debris. mCherry was excited using a 561-nm laser and the fluorescence measured using a 610/20-nm bandpass filter. Autofluorescence was determined using cells obtained from nontransgenic embryos using 488-nm excitation and measured using a 530/30-nm bandpass filter. The numbers of mCherry-positive cells were isolated by drawing a region on a two-parameter plot of mCherry versus autofluorescence just above the level of the autofluorescence. The number of mCherry-positive events was counted from 200,000 cells for each group. Experiments were performed in triplicate. The number of mCherry-positive cells was normalized to the uninjected group and the mean relative quantification was plotted.

Statistics

Statistical differences were evaluated using one-way ANOVA with the Newman–Keuls multiple comparison test. Statistics were calculated using GraphPad Prism version 5.0 software.

Results

Specific knockdown of zebrafish samhd1 causes a hindbrain-swelling phenotype

AGS5 is caused by loss-of-function mutations in the *SAMHD1* gene (5). As mutant *Samhd1* mice lack any overt physical phenotype (14, 15), we sought to investigate the use of zebrafish embryos as a possible alternative vertebrate disease model. A single *samhd1* ortholog (ENSDARG00000071288) can be identified in the zebrafish reference genome (zv9, www.ensembl.org). Zebrafish samhd1 protein (accession number NP_001153405, http://www.ncbi.nlm.nih.gov/protein/) is relatively well conserved, sharing 60% homology with the human ortholog (Supplemental Fig. 2). We performed *samhd1* gene knockdown experiments in WT zebrafish embryos using an antisense MO strategy. We designed an MO to specifically target the translation start codon (ATG) of the zebrafish *samhd1* transcript, which was predicted to inhibit protein synthesis. Using an anti-human SAMHD1 Ab, Western blot analyses confirmed a reduction in samhd1 protein expression in morphants in comparison with controls (Fig. 1A), thereby providing us with confidence that the MO was specifically limiting *samhd1* translation in vivo. We next monitored the effects of loss of *samhd1* during larval development. Following *samhd1* knockdown, we observed a mild developmental delay that we perceived to relate possibly to a nonspecific MO effect (25). However, we also observed swelling within the fourth ventricle of the brain between 2 and 3 dpf, a phenotype not normally reported with the use of MO technology. To account for variation in the severity of this phenotype, we classified swellings into four categories: normal, mild, moderate, and severe (Fig. 1B). Embryos were scored in n = 80–120 morphants and the same number of controls at 3 dpf; 94% of *samhd1* morphants displayed a severe (50% of total) or moderate (44% of total) swelling phenotype (Fig. 1C). To confirm whether this could be specifically attributed to loss of *samhd1*, we next coinjected human WT *SAMHD1* mRNA with the *samhd1* ATG

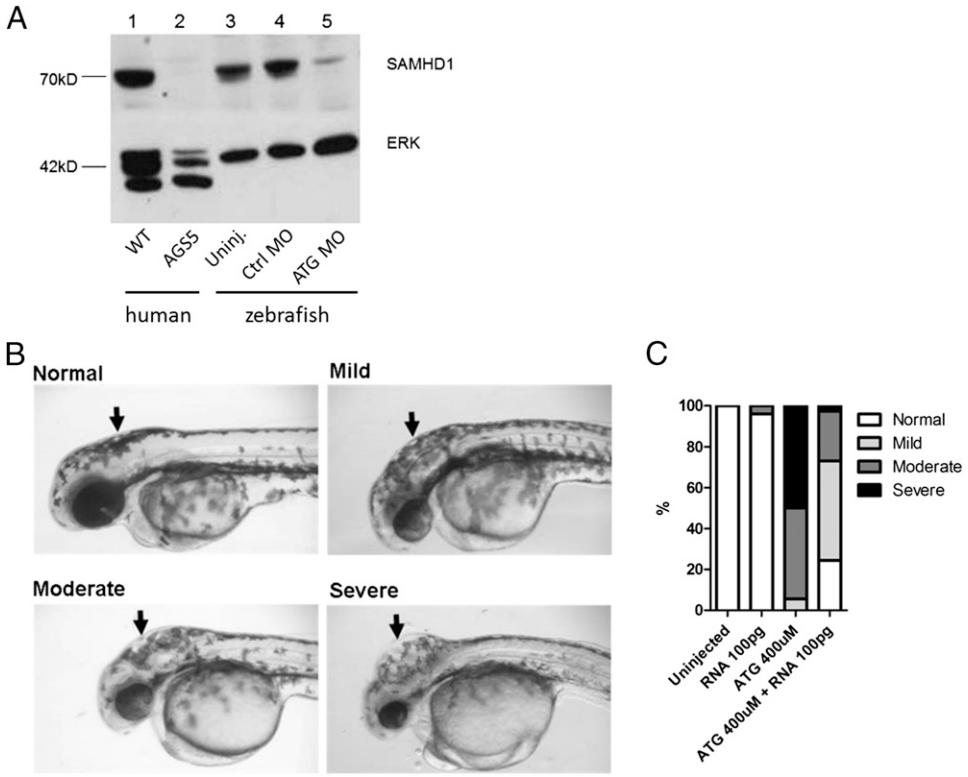

FIGURE 1. Specific knockdown of zebrafish *samhd1* is associated with hindbrain ventricular swelling. (**A**) Western blot analysis reveals a reduction in samhd1 protein level in *samhd1* ATG (*lane 5*) morphants in comparison with uninjected (*lane 3*) and control MO (*lane 4*) embryos (n = 40–60 embryos per group). WT human (*lane 1*) and *SAMHD1*-null AGS5 patient (*lane 2*) lymphoblastoid cell line lysates were also loaded as a specificity control for the anti-human SAMHD1 Ab. An anti-ERK Ab was used as a loading control. (**B**) Four levels of severity were categorized based on the hindbrain (fourth ventricle) swelling (arrow) phenotype observed between 2 and 3 dpf: normal, mild, moderate, and severe. Original magnification ×32. (**C**) Almost 100% of control embryos (uninjected and RNA only [100 pg] groups) exhibited normal brain development. Conversely, ~45% and 50% of embryos demonstrated moderate and severe brain swelling phenotypes when injected with the *samhd1* ATG MO (ATG 400 μM). The severity of this phenotype was reduced considerably when the *samhd1* ATG MO was coinjected with human *SAMHD1* RNA (ATG 400 μM plus RNA 100 pg; n = 40–80 embryos per group, repeated three times).

MO. Although, a generic developmental delay phenotype was retained, we recorded that only 2% of the coinjected embryos now exhibited severe swellings, whereas 24% and 49% displayed moderate and mild phenotypes, respectively (Fig. 1C). These rescue data suggest that the ventricular swelling observed is a direct result of specific knockdown of the *samhd1* gene.

Loss of samhd1 *is associated with a brain hemorrhage phenotype*

To gain insight into the cause of the cerebral swelling seen in *samhd1*-MO treated embryos, and considering the observation of a cerebral vasculopathy in patients with *SAMHD1* mutations (10–13), we next wanted to test whether there was any evidence that *samhd1* knockdown was associated with brain hemorrhage. We injected *samhd1* ATG MO into embryos derived from crossing a double transgenic *fli1*:GFP/*gata1*:DsRed reporter zebrafish line (19, 20). In these double-transgenic embryos, endothelial cells express GFP and erythrocytes express DsRed, allowing us to monitor the status of blood circulation by fluorescence stereomicroscopic examination of live animals. As a positive control, we examined *cecr1* morphants, because mutations in the *CECR1* gene cause an early-onset vasculopathy and knockdown of the zebrafish homolog is associated with brain hemorrhage (23). Embryos were quantified in six independent experiments for the presence or absence of blood pools within brain or head regions between 2 and 3 dpf (Fig. 2A). Knockdown of *cecr1* caused brain hemorrhage in 55.9% of injected embryos. Hemorrhages were observed in a comparable proportion of *samhd1* morphant embryos (46.7%), significantly higher in comparison with either uninjected (16.3%) or control morphant (20.3%) embryos (Fig. 2B). Thus, *samhd1* knockdown results in brain bleeding in zebrafish.

In addition, hindbrain swellings were quantified in triplicate experiments in *samhd1*, *cecr1*, control MO, and uninjected embryos at 2 dpf (Fig. 2C). Although a higher proportion of embryos displaying swellings were observed in *cecr1* (11.7% ± 2.8; mean ± SEM) morphants in comparison with the control MO group (1.2% ± 0.5), this difference was not significant. In contrast, the proportion of embryos exhibiting swellings was significantly higher in the *samhd1* morphant group (68.8% ± 7.7) compared with all other groups. This result suggests that the hindbrain swelling that we observed was specific for loss of *samhd1*, and not secondary to the disruption of cerebral vasculature.

Knockdown of samhd1 is associated with increased expression of genes involved in innate immune responses

Biochemically, AGS is characterized by a significant increase in ISG expression in peripheral blood (2). Recently, a transcriptional response has been described for larval zebrafish in response to infection from two different viruses (18). Although the repertoire of upregulated genes was distinct in response to the two infections, a degree of genetic overlap was shown to exist between both models. To assess whether the phenotype that we observed on knockdown of *samhd1* might be associated with increased transcription of innate immune-related genes, we measured the expression levels of a number of genes considered to play a role in antiviral, innate immune mechanisms in our *samhd1* morphant model. We established a panel of nine genes based on a combination of 1) preliminary *samhd1* morphant microarray data (data

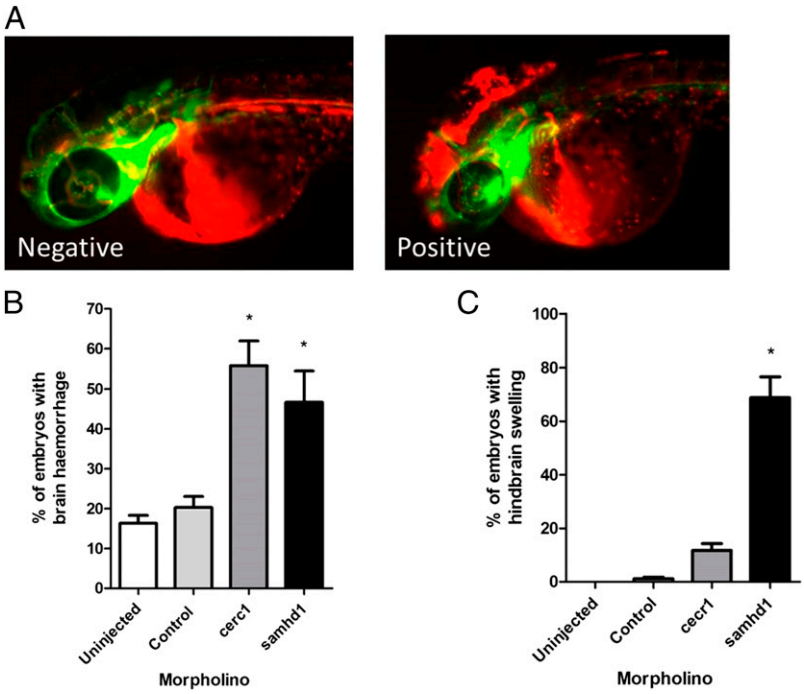

FIGURE 2. *samhd1* knockdown is associated with a brain hemorrhage phenotype in a proportion of morphants. (**A**) Examples of brain hemorrhage phenotypes in embryos (aged between 2 and 3 dpf) derived from a transgenic *fli1*:GFP/*gata1*:DsRed reporter zebrafish line. Embryos were scored as negative (*left panel*) or positive (*right panel*) for bleeding depending on the absence or presence of blood pooling (red fluorescent signal) within the head–brain regions, respectively. Original magnification ×50. (**B**) The proportion of embryos exhibiting brain hemorrhages was quantified for groups of embryos injected with *cecr1* or *samhd1* ATG MO in comparison with uninjected and control morphants. Brain hemorrhage was observed in a significantly higher proportion of *cecr1* (55.9%) and *samhd1* (46.7%) morphants, in comparison with uninjected (16.3%) and control morphants (20.3%; n = 30–80 embryos per group, repeated six times). (**C**) The percentage of hindbrain swellings was quantified in uninjected, control MO, *cecr1*, and *samhd1* ATG morphant embryos at 2 dpf. A significantly greater proportion of embryos exhibiting swellings were observed in the *samhd1* morphant group in comparison with any other group (n = 80–120 embryos per group, repeated three times). *$p < 0.05$ using one-way ANOVA with Newman–Keuls multiple comparison test.

not shown), 2) genes described as upregulated in zebrafish models of viral infection (18), and 3) ISGs defined as overexpressed in the context of human AGS (2). We performed Taqman QRT-PCR using specific probes designed to target each of these genes on cDNA synthesized from RNA that we harvested from n = 50–100 larvae per group at 4 dpf. We observed a significant increase in the expression of these genes in the *samhd1* ATG morphants (median RQ = 7.15; interquartile range (IQR) = 4.97–11.57) in comparison with *cecr1* morphants (median RQ = 1.88; IQR = 1.22–2.03), uninjected embryos (median RQ = 1.20; IQR = 1.02–1.39), and control morphants (median RQ = 1; baseline reference; Fig. 3). To confirm this result, we also used a second MO that targets the splice donor site at the intron–exon boundary of exon 4 of *samhd1* premRNA (Supplemental Fig. 3A), and we observed a significant increase in the expression of our gene panel (median RQ = 9.7; IQR = 6.77–17.05) in comparison with *cecr1* morphants and uninjected and control morphant embryos (Fig. 3).

Characterization of genes that can be considered as bona fide antiviral "signature" genes has not been studied in zebrafish as extensively as in humans (26). Indeed, stimulus-dependent variations in the innate immune transcriptional response exist in zebrafish (18). As the panel of genes that we used was selected based on criteria relating to categories 1–3 described above, we next wanted to test the validity of this result using an alternative zebrafish model of disturbed innate immunity. Hypomorphic mutations in the *ADAR* gene cause AGS6, and they are associated with a substantial upregulation of ISG expression (7). Mice lacking the *Adar* gene die in utero and similarly demonstrate a marked overexpression of ISGs (27, 28). According to the current version of the zebrafish reference genome (zv9), zebrafish have a unique *adar* ortholog (ENSDARG00000012389), previously identified (29) but not studied functionally. Using ATG and splice-blocking (exon 4) MOs to target *adar*, we observed a severe developmental phenotype even at low concentrations of the ATG MO. Conversely, *adar* splice morphants appeared morphologically normal at high MO concentrations, although it targets an exon used in all known splice variants of *adar*. RT-PCR of *adar* splice morphant cDNA, using primers that flank exon 4, confirmed aberrant splicing of the *adar* transcript (Supplemental Fig. 3B). RNA was harvested from n = 50–100 *adar* morphant embryos, and cDNA was synthesized before performing Taqman QRT-PCR using the probe set described above. We observed a significant increase in the expression of the innate immune genes included in our panel in *adar* ATG morphants (median RQ = 9.99; IQR = 6.04–29.31) in comparison with *cecr1* morphants and uninjected and control morphant embryos (Fig. 3). Overall, gene expression was not significantly altered in the *adar* splice morphants (median RQ = 2.37; IQR = 2.25–24.01) in comparison with controls, although expression of three of the nine genes was upregulated (*irf7*, *isg15*, and *stat1b*), suggesting that these embryos display a degree of innate immune gene activation, albeit milder in comparison with the *adar* ATG and the *samhd1* morphants.

ifnphi1 *expression is enhanced in response to samhd1 inhibition*

As well as a significant enhancement of ISG transcription, AGS is characterized molecularly by increased IFN-α activity in patient cerebrospinal fluid and serum (1, 2). In zebrafish, four type I IFNs are expressed (IFN-φ 1–4). However, only IFN-φ1 and IFN-φ3 are functional during larval development (30). We took advantage of

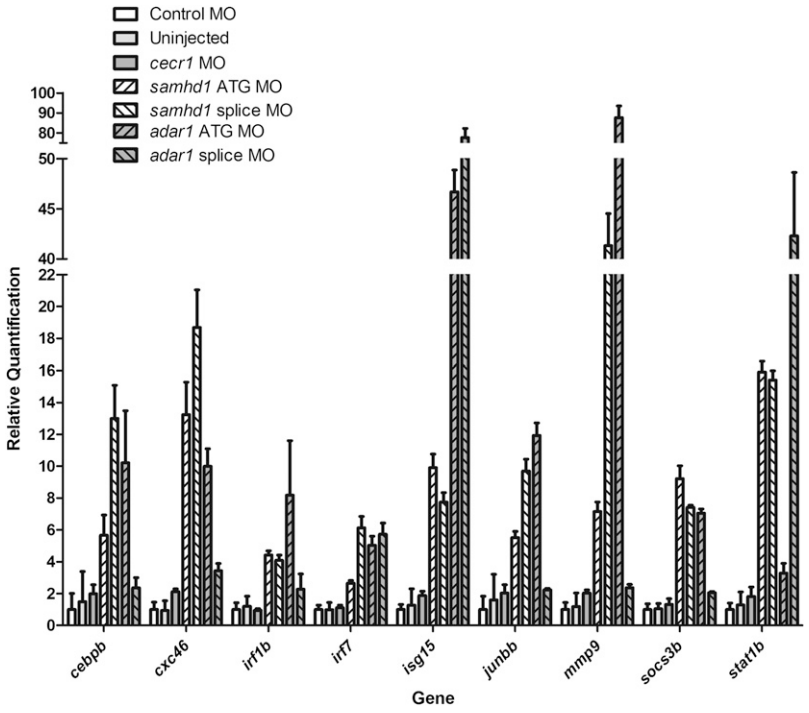

FIGURE 3. Taqman QRT-PCR was performed on cDNA synthesized from total RNA harvested from uninjected, control MO, *cecr1*, *samhd1* ATG, *samhd1* splice, and *adar* ATG and *adar* splice morphant embryos (n = 50–100 per group). The relative abundance (RQ) of target transcripts *cebpb*, *cxc46*, *irf1b*, *irf7*, *isg15*, *junbb*, *mmp9*, *socs3b*, and *stat1b* was normalized to the expression of the housekeeping gene *hprt1*. Each PCR was performed three times in triplicate per cDNA sample (total of nine technical repeats per sample). Biological repeats were also performed showing comparable differences (data not shown). A significant increase in expression of the nine genes was observed when comparing both *samhd1* ATG and splice morphants to controls and when comparing *adar* ATG morphants to controls, $p < 0.05$ using one-way ANOVA with Newman–Keuls multiple comparison test.

the transgenic *ifnphi1*:mCherry reporter line, embryos of which exhibit increased expression of mCherry in a subset of cells following viral infection, reflecting endogenous *ifnphi1* expression (21). To determine whether the increase in expression of our putative immune gene panel in the *samhd1* morphants was also associated with upregulation of *ifnphi1* itself, we performed *samhd1* knockdown experiments in zebrafish embryos harvested from the transgenic *ifnphi1*:mCherry reporter line. At 4 dpf, morphant embryos were analyzed by fluorescent microscopy and subsequently processed for flow cytometry and quantification of mCherry-positive cells. We observed significant increases in the number of mCherry-positive cells in both *samhd1* ATG (RQ = 2.92 ± 0.5; mean ± SEM) and *samhd1* splice morphants (RQ = 4.20 ± 0.1) in comparison with control morphants (RQ = 1.40 ± 0.2) and uninjected larvae (median RQ = 1; baseline reference; Fig. 4). Furthermore, we also recorded a significant increase in mCherry-positive cells in *adar* splice morphants (RQ = 2.44 ± 0.1), suggesting an increase in innate immune gene expression with upregulation of *ifnϕ1* in both models.

Discussion

Mice deficient in the genes associated with AGS1-7 exist. However, the suitability of these models to study the inflammatory and neurological aspects of AGS is restricted, either because of a lack of brain phenotype—such as *Trex1* (31–33), *Samhd1* (14, 15), or *Ifih1* (34)—or because of embryonic lethality—such as *Rnaseh2* (35, 36) and *Adar* (27, 28). To develop treatments for AGS patients, it is desirable to generate an animal model that reliably recapitulates the neurological characteristic aspects of the disease. In this study, we describe a novel in vivo model of AGS demonstrating, to our knowledge for the first time, inflammatory and brain phenotypes that may be relevant to the human condition.

Following knockdown of the *samhd1* gene in zebrafish embryos, we observed hindbrain ventricular swellings and hemorrhages in the brain. In addition to the severe brain damage, likely occurring secondary to a microangiopathic process, which is common to all forms of AGS, *SAMHD1* mutations also result in an apparently gene-specific cerebral vasculopathic phenotype frequently leading to intracerebral hemorrhage during early life (10–13). As with all subtypes of the disorder, AGS5 is associated with a significant upregulation of ISGs (2). Likewise, increased expression of ISGs was observed in spleen, fibroblasts, and macrophages harvested from mice lacking the *Samhd1* gene (14, 15). However, these mice did not display any detectable brain, or any other, phenotype. Our data imply that zebrafish might be a better model for studying AGS5-related cerebrovascular defects, either because zebrafish samhd1 shares a greater degree of functionality with the human ortholog in comparison with the mouse protein, or, because of some form of compensatory genetic mechanism in mice, which is absent in zebrafish. Such conclusions are speculative at this point, in part because of differences between the models regarding transient gene knockdown versus germline mutation.

Loss of *cecr1* in zebrafish is associated with a brain hemorrhage phenotype (23). In contrast to *samhd1* knockdown, however, we did not detect hindbrain ventricular swellings in this model. Brain hemorrhages and hindbrain ventricular swelling have been recorded together as a result of endothelial defects in zebrafish models of *pak2a* deficiency (37, 38). Further study is required to determine the cellular processes associated with the features seen in our *samhd1* morphants.

The ISG response in humans is characterized by differences in the gene transcriptional profile induced according to the viral stimulus involved (26). The ISG innate immune transcriptional response to different viral stimulation in zebrafish is yet to be fully defined, although it is apparent that overlap exists with the human state (18). Of note, as in humans, it appears that the transcriptional response in fish is stimulus dependent (18, 30, 39). Against this background, we selected a panel of transcripts that might be relevant to a putative innate immune response as observed in humans secondary to AGS-related protein loss.

Using data obtained from a preliminary microarray expression analysis, in combination with knowledge of genes significantly upregulated in zebrafish models of viral infection (18) and in human AGS (2), we compiled a panel of innate immune genes to test in our zebrafish model. We observed significantly enhanced expression of these genes using two *samhd1*-targeting strategies. In addition, we recorded upregulation of these transcripts in *adar* morphants (AGS6),

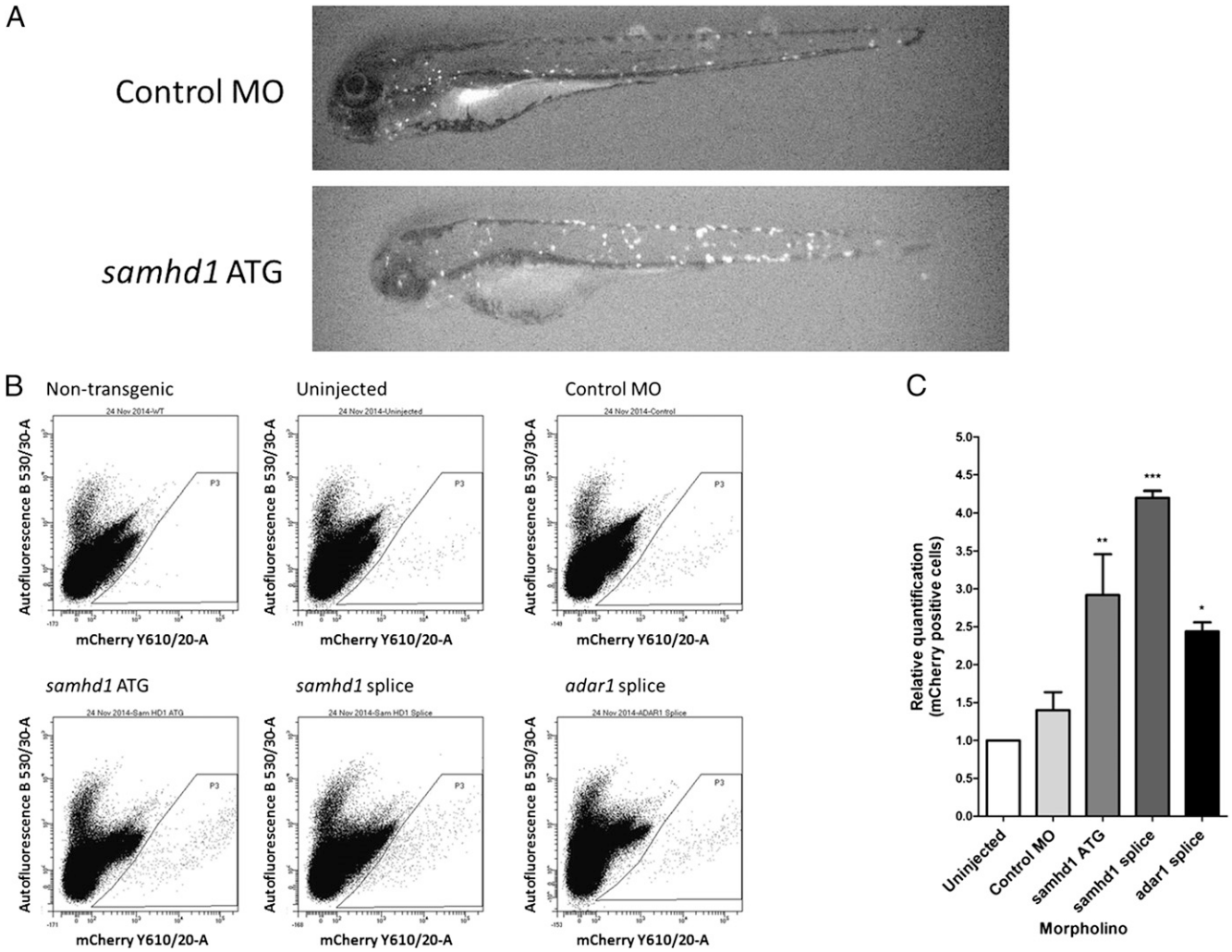

FIGURE 4. Inhibition of the *samhd1* gene is associated with an increase in *ifnphi1* expression. (**A**) Example of the enhanced numbers of mCherry-positive cells distributed throughout the body in *ifnphi1:*mCherry transgenic embryos injected with *samhd1* MO (*lower panel*) in comparison with controls (*upper panel*). Original magnification ×32. (**B**) Representative two-parameter scatter plots of mCherry-positive cells analyzed from single-cell suspensions generated from *ifnphi1:*mCherry embryos from uninjected, control MO, *samhd1* ATG, *samhd1* splice, and *adar* splice morphant groups. (**C**) A significant increase in the relative number of *ifnphi1*-expressing cells was observed in *samhd1* and *adar* morphants in comparison with controls following flow cytometry quantification of mCherry-positive cells. The number of mCherry-positive cells counted from P3 was normalized to the uninjected group for each run, and the mean relative quantification was plotted ($n = 40$–60 embryos per group, repeated three times). *$p < 0.05$, **$p < 0.01$, ***$p < 0.001$ using one-way ANOVA with Newman–Keuls multiple comparison test.

which we performed to validate the selection of the genes in our panel. Taken together, these data suggest that, as for mammals, *samhd1* and *adar* possess functions that involve regulation of innate immune responses in zebrafish.

The gene, *isg15*, was highlighted as significantly upregulated in our preliminary studies and subsequently confirmed following QRT-PCR. In humans, *ISG15* dysregulation is associated with neuroinflammatory disease (2, 40). Zebrafish *isg15* is also activated after viral stimulation (18), and it has been shown to be a key regulator of IFN-mediated antiviral responses (41). In addition, we observed upregulation of *mmp9* and *junbb*, both of which are induced in zebrafish viral infection models (18). Functional knowledge of the zebrafish specific chemokine *cxc46* is relatively poor. However, other CXC chemokine family members are upregulated in response to viral infection in zebrafish larvae (18), and increased expression of chemokines has been reported in AGS (42, 43). Increased expression of genes encoding the transcription factors irf1b, irf7, stat1b, and cebpb, as observed in our morphants, has also been recorded following exposure to two viruses in zebrafish infection models (18), and significant upregulation of the human orthologs, *STAT1* and *IRF7* is seen in AGS (7). Although not implicated in AGS or zebrafish viral infection models, we deemed the *socs3b* gene worthy of further examination because of the known inflammatory-related functions of the suppressors of cytokines (SOCS) proteins, and the observation of increased *socs3* expression in carp following infection with Spring viremia of carp virus (39). Importantly, consistent with an upregulation of ISGs and innate immune genes, we were also able to demonstrate increased expression of the zebrafish type I IFN, *ifnphi1*, following knockdown of *samhd1* and *adar*.

In conclusion, we have observed that the loss of *samhd1* in zebrafish is associated with features reminiscent of the cerebral hemorrhage phenotype in AGS5, and that both *samhd1* and *adar* zebrafish knockdown recapitulate the IFN response seen in AGS. Even taking into account concerns over the use of MO technology in zebrafish (25), our data indicate that the analysis of stable mutants of *samhd1* and *adar* in zebrafish is warranted to shed light on the nature of the innate immune stimulus in

these disease states, and to extend our knowledge of antiviral responses in zebrafish more generally.

Acknowledgments

We thank Dr. Adam Hurlstone and Dr. Shane Herbert for sharing zebrafish strains and equipment and Mike Jackson at the University of Manchester Flow Cytometry Facility for technical support.

Disclosures

The authors have no financial conflicts of interest.

References

1. Lebon, P., J. Badoual, G. Ponsot, F. Goutières, F. Hémeury-Cukier, and J. Aicardi. 1988. Intrathecal synthesis of interferon-alpha in infants with progressive familial encephalopathy. *J. Neurol. Sci.* 84: 201–208.
2. Rice, G. I., G. M. Forte, M. Szynkiewicz, D. S. Chase, A. Aeby, M. S. Abdel-Hamid, S. Ackroyd, R. Allcock, K. M. Bailey, U. Balottin, et al. 2013. Assessment of interferon-related biomarkers in Aicardi-Goutières syndrome associated with mutations in TREX1, RNASEH2A, RNASEH2B, RNASEH2C, SAMHD1, and ADAR: a case-control study. *Lancet Neurol.* 12: 1159–1169.
3. Crow, Y. J., B. E. Hayward, R. Parmar, P. Robins, A. Leitch, M. Ali, D. N. Black, H. van Bokhoven, H. G. Brunner, B. C. Hamel, et al. 2006. Mutations in the gene encoding the 3′-5′ DNA exonuclease TREX1 cause Aicardi-Goutières syndrome at the AGS1 locus. *Nat. Genet.* 38: 917–920.
4. Crow, Y. J., A. Leitch, B. E. Hayward, A. Garner, R. Parmar, E. Griffith, M. Ali, C. Semple, J. Aicardi, R. Babul-Hirji, et al. 2006. Mutations in genes encoding ribonuclease H2 subunits cause Aicardi-Goutières syndrome and mimic congenital viral brain infection. *Nat. Genet.* 38: 910–916.
5. Rice, G. I., J. Bond, A. Asipu, R. L. Brunette, I. W. Manfield, I. M. Carr, J. C. Fuller, R. M. Jackson, T. Lamb, T. A. Briggs, et al. 2009. Mutations involved in Aicardi-Goutières syndrome implicate SAMHD1 as regulator of the innate immune response. *Nat. Genet.* 41: 829–832.
6. Rice, G. I., Y. del Toro Duany, E. M. Jenkinson, G. M. Forte, B. H. Anderson, G. Ariaudo, B. Bader-Meunier, E. M. Baildam, R. Battini, M. W. Beresford, et al. 2014. Gain-of-function mutations in IFIH1 cause a spectrum of human disease phenotypes associated with upregulated type I interferon signaling. *Nat. Genet.* 46: 503–509.
7. Rice, G. I., P. R. Kasher, G. M. Forte, N. M. Mannion, S. M. Greenwood, M. Szynkiewicz, J. E. Dickerson, S. S. Bhaskar, M. Zampini, T. A. Briggs, et al. 2012. Mutations in ADAR1 cause Aicardi-Goutières syndrome associated with a type I interferon signature. *Nat. Genet.* 44: 1243–1248.
8. Goldstone, D. C., V. Ennis-Adeniran, J. J. Hedden, H. C. Groom, G. I. Rice, E. Christodoulou, P. A. Walker, G. Kelly, L. F. Haire, M. W. Yap, et al. 2011. HIV-1 restriction factor SAMHD1 is a deoxynucleoside triphosphate triphosphohydrolase. *Nature* 480: 379–382.
9. Lahouassa, H., W. Daddacha, H. Hofmann, D. Ayinde, E. C. Logue, L. Dragin, N. Bloch, C. Maudet, M. Bertrand, T. Gramberg, et al. 2012. SAMHD1 restricts the replication of human immunodeficiency virus type 1 by depleting the intracellular pool of deoxynucleoside triphosphates. *Nat. Immunol.* 13: 223–228.
10. du Moulin, M., P. Nürnberg, Y. J. Crow, and F. Rutsch. 2011. Cerebral vasculopathy is a common feature in Aicardi-Goutieres syndrome associated with SAMHD1 mutations. *Proc. Natl. Acad. Sci. USA* 108: E232–, author reply E233.
11. Ramesh, V., B. Bernardi, A. Stafa, C. Garone, E. Franzoni, M. Abinun, P. Mitchell, D. Mitra, M. Friswell, J. Nelson, et al. 2010. Intracerebral large artery disease in Aicardi-Goutières syndrome implicates SAMHD1 in vascular homeostasis. *Dev. Med. Child Neurol.* 52: 725–732.
12. Thiele, H., M. du Moulin, K. Barczyk, C. George, W. Schwindt, G. Nürnberg, M. Frosch, G. Kurlemann, J. Roth, P. Nürnberg, and F. Rutsch. 2010. Cerebral arterial stenoses and stroke: novel features of Aicardi-Goutières syndrome caused by the Arg164X mutation in SAMHD1 are associated with altered cytokine expression. *Hum. Mutat.* 31: E1836–E1850.
13. Xin, B., S. Jones, E. G. Puffenberger, C. Hinze, A. Bright, H. Tan, A. Zhou, G. Wu, J. Vargus-Adams, D. Agamanolis, and H. Wang. 2011. Homozygous mutation in SAMHD1 gene causes cerebral vasculopathy and early onset stroke. *Proc. Natl. Acad. Sci. USA* 108: 5372–5377.
14. Behrendt, R., T. Schumann, A. Gerbaulet, L. A. Nguyen, N. Schubert, D. Alexopoulou, U. Berka, S. Lienenklaus, K. Peschke, K. Gibbert, et al. 2013. Mouse SAMHD1 has antiretroviral activity and suppresses a spontaneous cell-intrinsic antiviral response. *Cell Reports* 4: 689–696.
15. Rehwinkel, J., J. Maelfait, A. Bridgeman, R. Rigby, B. Hayward, R. A. Liberatore, P. D. Bieniasz, G. J. Towers, L. F. Moita, Y. J. Crow, et al. 2013. SAMHD1-dependent retroviral control and escape in mice. *EMBO J.* 32: 2454–2462.
16. Renshaw, S. A., and N. S. Trede. 2012. A model 450 million years in the making: zebrafish and vertebrate immunity. *Dis. Model. Mech.* 5: 38–47.
17. van der Vaart, M., H. P. Spaink, and A. H. Meijer. 2012. Pathogen recognition and activation of the innate immune response in zebrafish. *Adv. Hematol.* 2012: 159807.
18. Briolat, V., L. Jouneau, R. Carvalho, N. Palha, C. Langevin, P. Herbomel, O. Schwartz, H. P. Spaink, J. P. Levraud, and P. Boudinot. 2014. Contrasted innate responses to two viruses in zebrafish: insights into the ancestral repertoire of vertebrate IFN-stimulated genes. *J. Immunol.* 192: 4328–4341.
19. Lawson, N. D., and B. M. Weinstein. 2002. In vivo imaging of embryonic vascular development using transgenic zebrafish. *Dev. Biol.* 248: 307–318.
20. Traver, D., B. H. Paw, K. D. Poss, W. T. Penberthy, S. Lin, and L. I. Zon. 2003. Transplantation and in vivo imaging of multilineage engraftment in zebrafish bloodless mutants. *Nat. Immunol.* 4: 1238–1246.
21. Palha, N., F. Guivel-Benhassine, V. Briolat, G. Lutfalla, M. Sourisseau, F. Ellett, C. H. Wang, G. J. Lieschke, P. Herbomel, O. Schwartz, and J. P. Levraud. 2013. Real-time whole-body visualization of Chikungunya Virus infection and host interferon response in zebrafish. *PLoS Pathog.* 9: e1003619.
22. Kimmel, C. B., W. W. Ballard, S. R. Kimmel, B. Ullmann, and T. F. Schilling. 1995. Stages of embryonic development of the zebrafish. *Dev. Dyn.* 203: 253–310.
23. Zhou, Q., D. Yang, A. K. Ombrello, A. V. Zavialov, C. Toro, A. V. Zavialov, D. L. Stone, J. J. Chae, S. D. Rosenzweig, K. Bishop, et al. 2014. Early-onset stroke and vasculopathy associated with mutations in ADA2. *N. Engl. J. Med.* 370: 911–920.
24. Kasher, P. R., Y. Namavar, P. van Tijn, K. Fluiter, A. Sizarov, M. Kamermans, A. J. Grierson, D. Zivkovic, and F. Baas. 2011. Impairment of the tRNA-splicing endonuclease subunit 54 (tsen54) gene causes neurological abnormalities and larval death in zebrafish models of pontocerebellar hypoplasia. *Hum. Mol. Genet.* 20: 1574–1584.
25. Schulte-Merker, S., and D. Y. Stainier. 2014. Out with the old, in with the new: reassessing morpholino knockdowns in light of genome editing technology. *Development* 141: 3103–3104.
26. Schoggins, J. W., S. J. Wilson, M. Panis, M. Y. Murphy, C. T. Jones, P. Bieniasz, and C. M. Rice. 2011. A diverse range of gene products are effectors of the type I interferon antiviral response. *Nature* 472: 481–485.
27. Hartner, J. C., C. R. Walkley, J. Lu, and S. H. Orkin. 2009. ADAR1 is essential for the maintenance of hematopoiesis and suppression of interferon signaling. *Nat. Immunol.* 10: 109–115.
28. Mannion, N. M., S. M. Greenwood, R. Young, S. Cox, J. Brindle, D. Read, C. Nellåker, C. Vesely, C. P. Ponting, P. J. McLaughlin, et al. 2014. The RNA-editing enzyme ADAR1 controls innate immune responses to RNA. *Cell Reports* 9: 1482–1494.
29. Slavov, D., T. Crnogorac-Jurcević, M. Clark, and K. Gardiner. 2000. Comparative analysis of the DRADA A-to-I RNA editing gene from mammals, pufferfish and zebrafish. *Gene* 250: 53–60.
30. Langevin, C., E. Aleksejeva, G. Passoni, N. Palha, J. P. Levraud, and P. Boudinot. 2013. The antiviral innate immune response in fish: evolution and conservation of the IFN system. *J. Mol. Biol.* 425: 4904–4920.
31. Gall, A., P. Treuting, K. B. Elkon, Y. M. Loo, M. Gale, Jr., G. N. Barber, and D. B. Stetson. 2012. Autoimmunity initiates in nonhematopoietic cells and progresses via lymphocytes in an interferon-dependent autoimmune disease. *Immunity* 36: 120–131.
32. Morita, M., G. Stamp, P. Robins, A. Dulic, I. Rosewell, G. Hrivnak, G. Daly, T. Lindahl, and D. E. Barnes. 2004. Gene-targeted mice lacking the Trex1 (DNase III) 3′—>5′ DNA exonuclease develop inflammatory myocarditis. *Mol. Cell. Biol.* 24: 6719–6727.
33. Stetson, D. B., J. S. Ko, T. Heidmann, and R. Medzhitov. 2008. Trex1 prevents cell-intrinsic initiation of autoimmunity. *Cell* 134: 587–598.
34. Funabiki, M., H. Kato, Y. Miyachi, H. Toki, H. Motegi, M. Inoue, O. Minowa, A. Yoshida, K. Deguchi, H. Sato, et al. 2014. Autoimmune disorders associated with gain of function of the intracellular sensor MDA5. *Immunity* 40: 199–212.
35. Hiller, B., M. Achleitner, S. Glage, R. Naumann, R. Behrendt, and A. Roers. 2012. Mammalian RNase H2 removes ribonucleotides from DNA to maintain genome integrity. *J. Exp. Med.* 209: 1419–1426.
36. Reijns, M. A., B. Rabe, R. E. Rigby, P. Mill, K. R. Astell, L. A. Lettice, S. Boyle, A. Leitch, M. Keighren, F. Kilanowski, et al. 2012. Enzymatic removal of ribonucleotides from DNA is essential for mammalian genome integrity and development. *Cell* 149: 1008–1022.
37. Buchner, D. A., F. Su, J. S. Yamaoka, M. Kamei, J. A. Shavit, L. K. Barthel, B. McGee, J. D. Amigo, S. Kim, A. W. Hanosh, et al. 2007. pak2a mutations cause cerebral hemorrhage in redhead zebrafish. *Proc. Natl. Acad. Sci. USA* 104: 13996–14001.
38. Liu, J., S. D. Fraser, P. W. Faloon, E. L. Rollins, J. Vom Berg, O. Starovic-Subota, A. L. Laliberte, J. N. Chen, F. C. Serluca, and S. J. Childs. 2007. A betaPix Pak2a signaling pathway regulates cerebral vascular stability in zebrafish. *Proc. Natl. Acad. Sci. USA* 104: 13990–13995.
39. Xiao, Z. G., H. Liu, J. P. Fu, W. Hu, Y. P. Wang, and Q. L. Guo. 2010. Cloning of common carp SOCS-3 gene and its expression during embryogenesis, GH-transgene and viral infection. *Fish Shellfish Immunol.* 28: 362–371.
40. Zhang, X., D. Bogunovic, B. Payelle-Brogard, V. Francois-Newton, S. D. Speer, C. Yuan, S. Volpi, Z. Li, O. Sanal, D. Mansouri, et al. 2015. Human intracellular ISG15 prevents interferon-α/β over-amplification and auto-inflammation. *Nature* 517: 89–93.
41. Langevin, C., L. M. van der Aa, A. Houel, C. Torhy, V. Briolat, A. Lunazzi, A. Harmache, M. Bremont, J. P. Levraud, and P. Boudinot. 2013. Zebrafish ISG15 exerts a strong antiviral activity against RNA and DNA viruses and regulates the interferon response. *J. Virol.* 87: 10025–10036.
42. Takanohashi, A., M. Prust, J. Wang, H. Gordish-Dressman, M. Bloom, G. I. Rice, J. L. Schmidt, Y. J. Crow, P. Lebon, T. W. Kuijpers, et al. 2013. Elevation of proinflammatory cytokines in patients with Aicardi-Goutières syndrome. *Neurology* 80: 997–1002.
43. van Heteren, J. T., F. Rozenberg, E. Aronica, D. Troost, P. Lebon, and T. W. Kuijpers. 2008. Astrocytes produce interferon-alpha and CXCL10, but not IL-6 or CXCL8, in Aicardi-Goutières syndrome. *Glia* 56: 568–578.